LBL-16902
Preprint c.2

Lawrence Berkeley Laboratory
UNIVERSITY OF CALIFORNIA

RECEIVED
LAWRENCE
BERKELEY LABORATORY

JAN 17 1984

LIBRARY AND
DOCUMENTS SECTION

To be submitted for publication

ON LINE CHARACTERIZATION OF HEAVY-ION BEAMS WITH SEMICONDUCTOR DETECTORS

J. Llacer, C.A. Tobias, W.R. Holley, and T. Kanai

September 1983

TWO-WEEK LOAN COPY

This is a Library Circulating Copy which may be borrowed for two weeks. For a personal retention copy, call Tech. Info. Division, Ext. 6782.

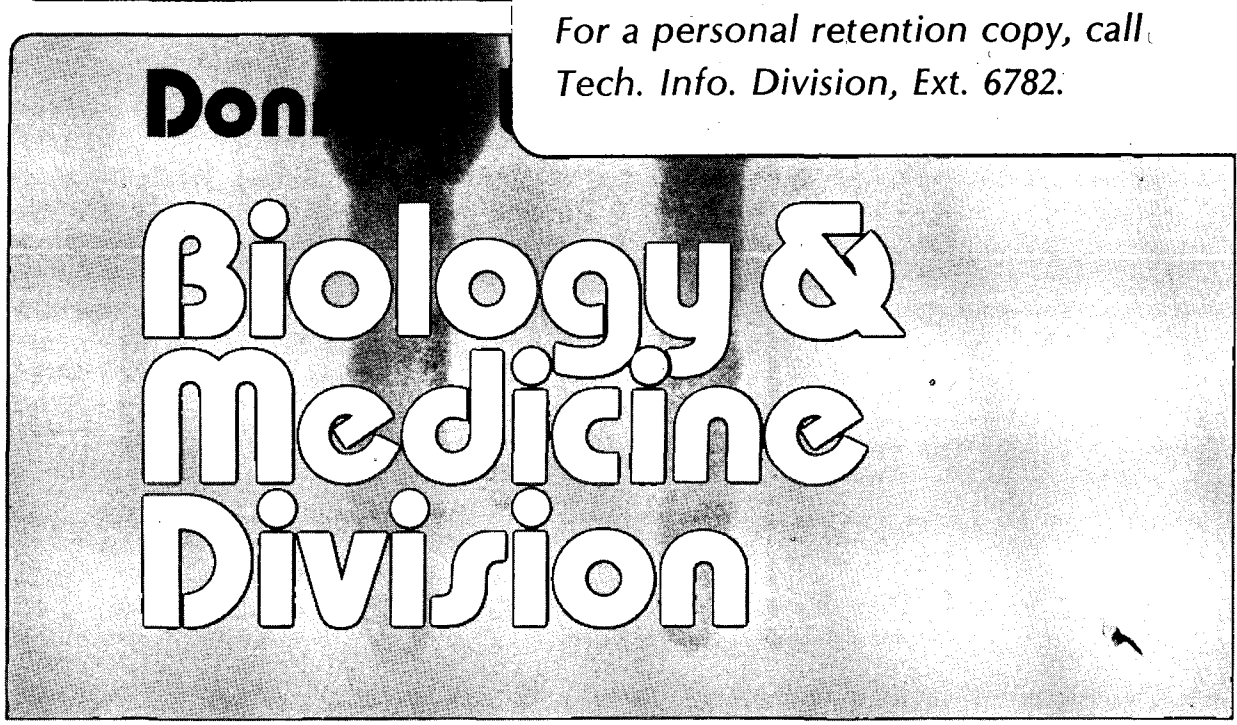

LBL-16902
c.2

Prepared for the U.S. Department of Energy under Contract DE-AC03-76SF00098

DISCLAIMER

This document was prepared as an account of work sponsored by the United States Government. While this document is believed to contain correct information, neither the United States Government nor any agency thereof, nor the Regents of the University of California, nor any of their employees, makes any warranty, express or implied, or assumes any legal responsibility for the accuracy, completeness, or usefulness of any information, apparatus, product, or process disclosed, or represents that its use would not infringe privately owned rights. Reference herein to any specific commercial product, process, or service by its trade name, trademark, manufacturer, or otherwise, does not necessarily constitute or imply its endorsement, recommendation, or favoring by the United States Government or any agency thereof, or the Regents of the University of California. The views and opinions of authors expressed herein do not necessarily state or reflect those of the United States Government or any agency thereof or the Regents of the University of California.

LBL-16902

ON LINE CHARACTERIZATION OF HEAVY-ION BEAMS WITH SEMICONDUCTOR DETECTORS

J. Llacer, C. A. Tobias, and W. R. Holley

Lawrence Berkeley Laboratory,
University of California,
Berkeley, California 94720

and

T. Kanai

National Institute of Radiological Sciences,
Chiba-shi 260, Japan

ABSTRACT

Heavy ion beams used in biomedical studies suffer a substantial amount of nuclear reactions (fragmentation) as they traverse matter. Since it has been demonstrated that dose and linear energy transfer (LET) are not a sufficient description of a beam for the purpose of understanding its biological effects, it is necessary to be able to separate the components of a complex beam so that their individual effects can be analyzed.

A simple and small assembly consisting of a thin silicon LET detector, in time coincidence with a thick germanium residual energy detector has been used in measurements of the components of Ne-20 and Si-28 high energy ion beams. The detector system can be placed at any experimental area without difficulty and it can carry out a beam analysis in a few minutes, making it very appropriate for fast on-line measurements and verification of beam characteristics.

LET values measured by the silicon detector agree well with results of the Bethe stopping power calculations, and the dose measured for the beam components can be used to obtain Bragg curves that are in good agreement with those obtained by ionization chamber measurements. The numbers and LET distribution of primaries and fragments at different positions of the Bragg curves, as well as fractional dose contributed by the different components are determined directly from the experimental data. Particle velocity distributions can be obtained for the higher Z fragments. Limitations and advantages of the simple measurement technique are discussed.

I. INTRODUCTION

Heavy ions are being used in a variety of basic and applied biomedical studies, including cell, tissue and organ radiobiology, cancer diagnosis (radiography), and therapy at the Lawrence Berkeley Laboratory. In the majority of cases, the pure heavy-ion beams delivered by the Bevalac accelerator do not have the characteristics of penetration depth, cross-sectional width, or Bragg peak width that are desired for a specific application. Metal foils, rotating or fixed ridge filters, and/or variable depth absorbers are then interposed between the beam delivery port and the subject of irradiation, generating a substantial number of fragment nuclei in the beam.

Fragmentation events are quite common for the particles and energies of interest in biomedical applications. Four types of fragmentation events are shown in Figure 1, which are photomicrographs of tracks in photographic emulsion: (a) A pure projectile fragmentation in which two heavy fragments (dense tracks) and two protons were produced; these are very rare events. (b) A pure projectile fragmentation in which multiple light fragments are generated; this type of event is more common. (c) Projectile fragmentation with target breakup. A 2 GeV/nucleon argon particle strikes a small nucleus and both breakup. This is an excellent example of transverse momentum transfer in a collision, with the projectile fragments undergoing a drastic collective deflection. The scale bar corresponds to 50 micrometers. Finally, (d) shows the catastrophic destruction of projectile and target nuclei. This is most incident high energy argon particle. The scale bar corresponds to 100 μm^{-1}. This kind of event would be very rare in soft tissues. In water, events of the second type and those in which one nucleus fragments into one particle which is still heavy and a number of light fragments are the most common reactions, as our measurements show below.

FRAGMENTATION

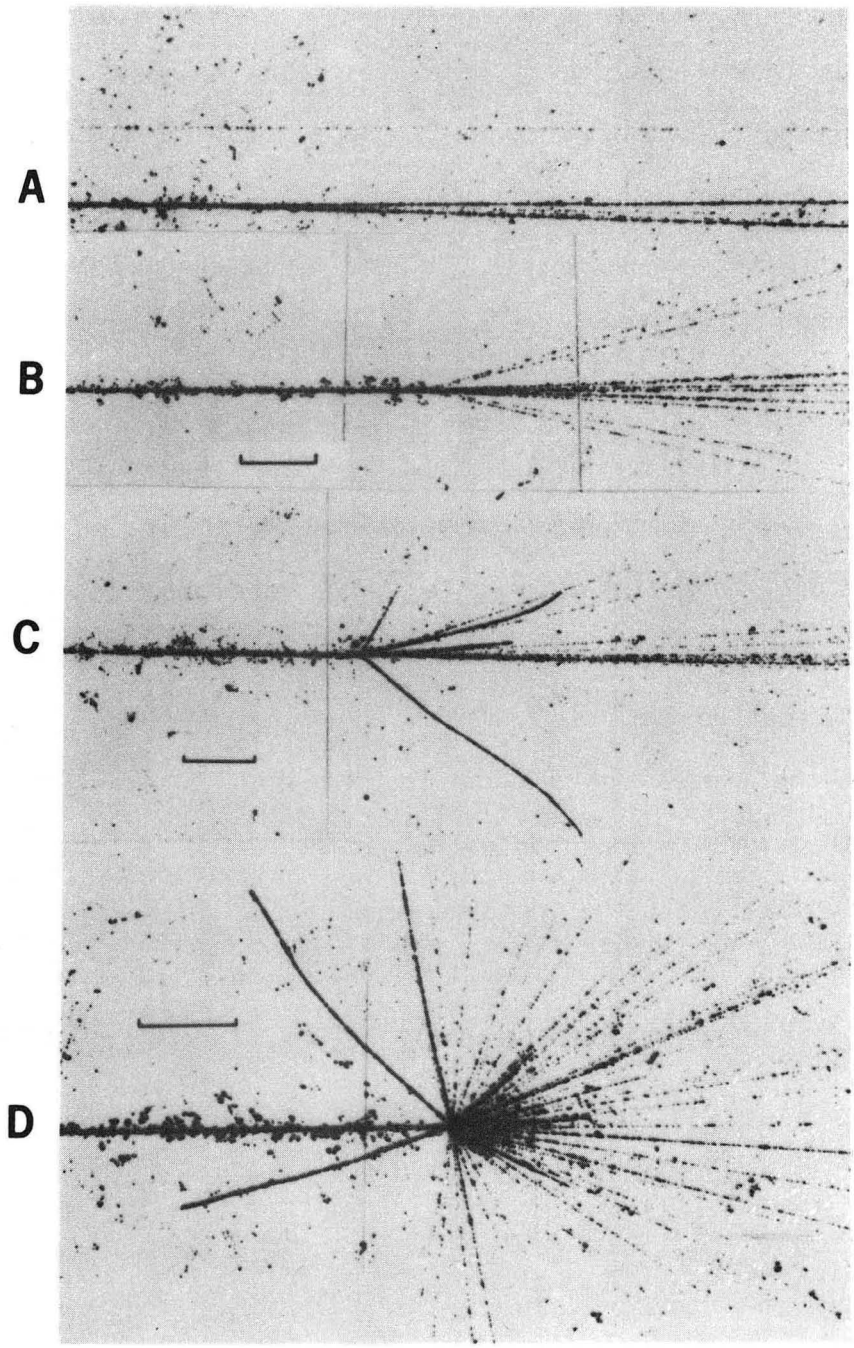

Figure 1
Heavy ion fragmentation effects. Four kinds of projectile and target fragmentation events: (a) and (b) are pure projectile fragmentation cases in which the beam particle breaks up into lighter particles; cases (c) and (d) show events in which a target nucleus also breaks up. (XBB 819-8965A)

Although we obtain reliable information routinely about the dose delivered to a subject under all the irradiation conditions encountered, there is no experimental detailed knowledge of which particles generate the delivered dose and the contribution by each type of fragment. Chatterjee et al.[2] have described the general characteristics of the complex beams that can be used for biomedical applications based on information obtained from cosmic-ray data. Studies by Blakely et al.[3] make use of calculated data for complex beams in order to understand the inactivation of human kidney cells in vitro by heavy-ion beams. These studies show that dose and LET alone are not sufficient descriptions of a beam for the purpose of understanding its biological effects. It is, therefore, necessary to be able to separate the components of a beam and its fragments so that the possibly different biological effects of each component can be accounted for.

Because the process of nuclear fragmentation becomes considerably more complex as the atomic number of the ion increases, it is not possible to calculate theoretically all the involved parameters. Although simplified theoretical calculations have been reported[4] which explain the shapes of measured Bragg curves in an approximate manner, the need for measurements of particle fragmentation is evident.

The analysis of particle tracks in photographic emulsion is an accurate way to study fragmentation. Jain showed in 1959[5] how heavy ions from cosmic radiation and their fragments could be identified in terms of the results of their interaction with the emulsion material. The technique has since been refined considerably[6,7] and that author is now carrying out the analysis of Bevalac heavy ion beams similar to the ones whose characteristics will be reported here.[8] Plastic detectors can also be used for the characterization of heavy ion beams in terms of LET and measurement of particle numbers vs. depth

of penetration[9,10,11] although the method does not allow a distinction between particles of different atomic charge if they have similar LET.

Characterization measurements of Bevalac beams with plastic detectors have recently been completed by Benton,[12] with results in the LET distributions in good agreement with the ones reported here. Although the emulsion method can give complete information about beam structure, it may take several days to process enough events to characterize one set of beam conditions. The more limited information obtainable from plastics can be made available to a beam user within several hours.

An extensive program exists at the Lawrence Berkeley Laboratory to provide detailed and accurate information on the fundamental nuclear processes occurring in the ion beams of biomedical interest[13,14] using time-of-flight methods and multidetector telescopes. The measurements carried out in that project require a dedicated beam line and a long processing time. We feel that a practical measurement method that can be used routinely in support of a biomedical research program should involve processing times of a few minutes and provide a biologist or a physician with reasonably accurate information about particle composition and dose contributed by each different nucleus in any of the large number of experimental configurations that can be set-up. The information does not need to separate different isotopes of a same element, for example, but it should be reliable and reproducible.

During investigations of the possible use of solid-state detectors for heavy-ion radiography and tomography[15] it became evident that detector configurations similar to the ones that were useful for those tasks were also applicable to beam quality analysis and could fulfill the requirements of speed indicated above. Fundamentally, a thin solid state detector (a few hundred micrometers of silicon), which can be considered to behave like a dense small

ionization chamber, measures the LET of traversing particles. A second thick detector (several centimeters of germanium) can then be used to measure the residual energy of particles. Knowledge of those two parameters can result in the identification of a particle's atomic charge. Although the process is not as precise as that of more complex detector arrangements, it appears possible to sacrifice some accuracy in favor of simplicity and ease of obtaining useful information. This paper will describe the detector and electronics configuration used for beam characterization experiments, discuss the methods of data analysis, and show the results of measurements with Ne-20 and Si-28 ion beams. A critical review of the data presented indicates both the advantages and disadvantages of the technique.

II. DETECTOR CHARACTERISTICS AND CONFIGURATION

Solid-state detectors exhibit three distinct characteristics which make them suitable for the purpose on hand: linearity, stability, and ease of calibration. The charge generated by ionizing radiation in the depletion region of a solid state detector is obtained from the expression

$$Q = E(eV) \times 1.6 \times 10^{-19} \text{ (coul)}/\varepsilon \text{ (eV)} \qquad (1)$$

where E is the energy deposited in the depletion region, and ε is the average ionization energy needed to create one electron-hole pair. The value of ε for silicon detectors at room temperature is 3.65 eV, and that of germanium at 77 K is 2.98 eV. These values depend principally on the band gap potential of the semiconductor material, which changes only by a few parts in 10^4 per ^{o}C of temperature change. The near constancy of ε

with changes in temperature accounts for the stability of solid-state detectors.

The value of ε is not totally independent of the rate of energy loss of the ionizing radiation in the detector material. For dense ionization tracks, as in the case of alpha particles, the effective values of ε are somewhat increased from the values given, due to recombination in the dense electron-hole plasma of the tracks. No definitive measurements of the dependence of ε with atomic charge Z and particle velocity have been carried out to date with heavy ions at the energies of interest for biomedical work. From work carried out for ions from neon to gold between energies of 5 to 160 MeV, stopping fully in a silicon surface barrier detector,[16] it is clear that a "pulse height defect" exists in those detectors. For Z=14, for example, the effect can be described by an increase in ε of 0.6%; we do not expect the magnitude of such variations to be important for our purposes until we measure ions much heavier than silicon.

The basic calibration procedure for solid state detectors is simple in principle. If a voltage step of magnitude V_{cal} is fed through a calibration capacitor C_{cal} to the input of a charge integrating amplifier, the charge delivered is

$$Q = C_{cal} \times V_{cal} \qquad (2)$$

provided that C_{cal} is much smaller than the input capacitance of the integrating amplifier. It is, therefore, possible to simulate particles that would deposit a given energy E into a depletion region of a detector by equating Equations (1) and (2), solving for V_{cal}, and delivering a voltage step of the correct magnitude to the C_{cal} of the preamplifier

circuits. In practice, a number of small cumulative errors in the procedure require that a reference source of ionizing radiation be used to establish an absolute calibration for a detector system.

We use the primary beam particles at the "plateau" region of their Bragg curve for that purpose. From their range, measured by ionization chambers and a variable water column absorber, we can calculate the energy and the rate of energy loss expected using standard methods. We can then establish a practical calibration for a particular beam. We consistently find differences between the "basic" and practical calibrations of less than 10%. We also need to change the calibration factors for a given beam at different ranges (different water absorber lengths) by a few percent in order for the calculated rates of energy loss for primary particles and the measured ones to coincide. A detailed analysis of those effects is beyond the scope of the present work.

Figure 2 shows schematically a typical measurement setup in one of the Bevatron experimental areas. A 0.44 cm water equivalent plastic scintillator is located near the beam port to count all the beam particles delivered during a measurement. We call this detector the upstream counter (UC). After the beam modifying equipment, the detector system is placed with the silicon detector at the position where the beam quality needs to be established. The inset of Figure 2 shows some details of the windows and detector configuration. The germanium detector is operated in vacuum, at liquid nitrogen temperature, while the silicon detector is in air, just outside the cryostat.

Figure 3 shows schematically the basic configuration of detectors and preamplifiers used in the experiments. The dE/dx (LET) detector consists of a 300 μm (approximately 586 μm water equivalent) thick silicon p-n

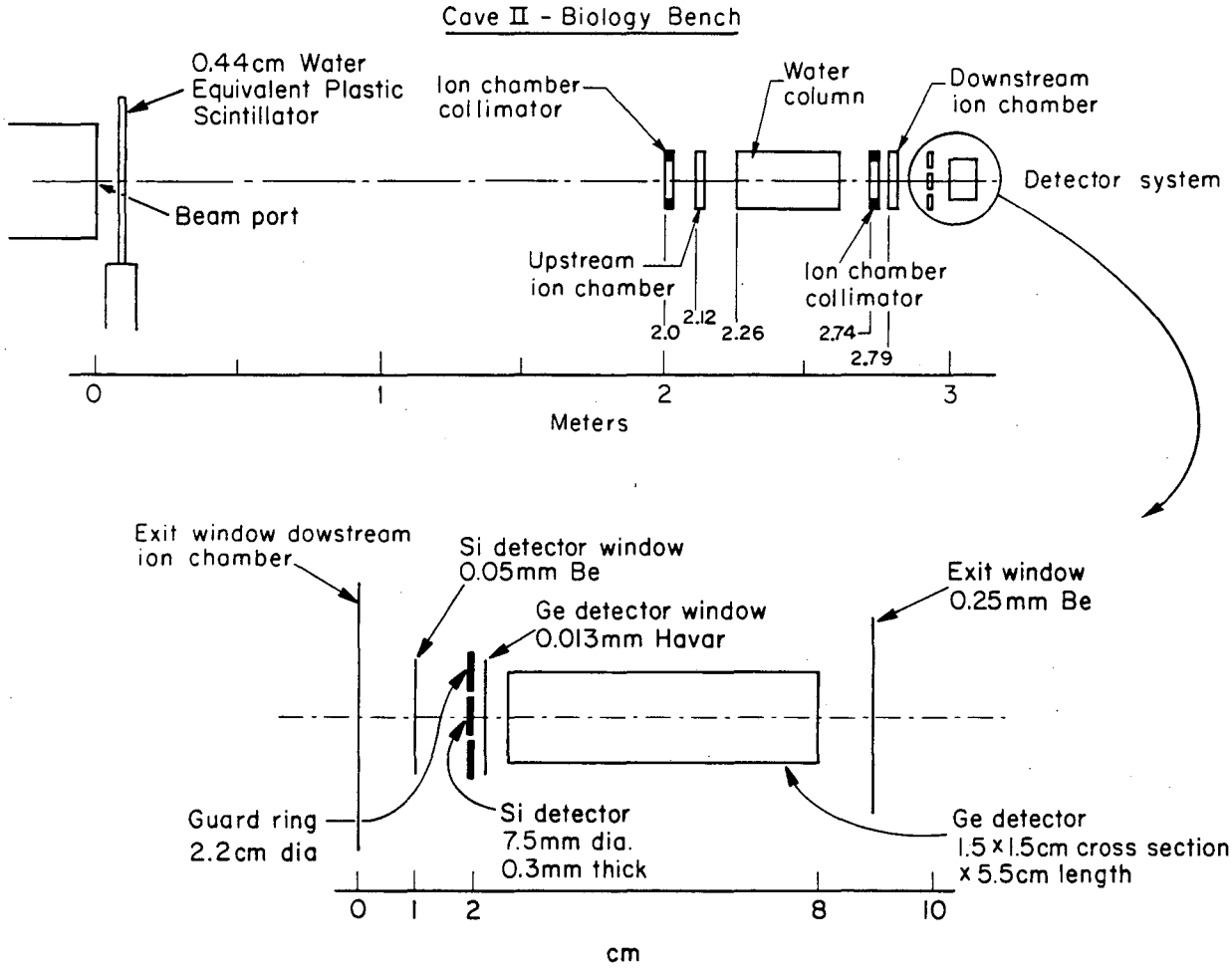

Figure 2
Schematic drawing of the experimental setup used in the measurements reported in this paper. The inset describes the detector system, with the windows for light and vacuum tightness. The germanium detector is kept in a cryostat, at liquid nitrogen temperature (77°K). (XBL 808-3609)

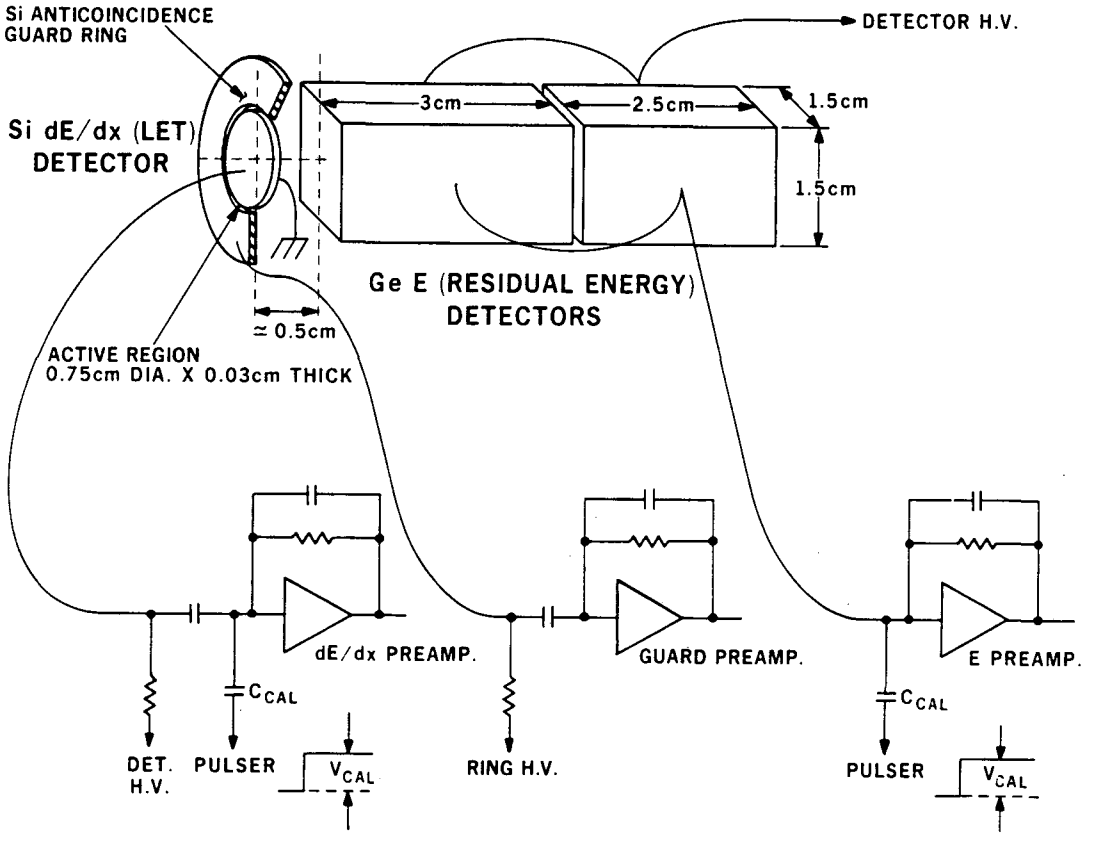

Figure 3
Schematic description of the silicon-germanium detector system for beam characterization. A thin silicon dE/dx detector measures LET and is followed by a thick germanium detector which measures residual energy. The two parameters can identify the atomic number of a particle in most cases. An anticoincidence guard ring in the silicon detector defines the active region and prevents pile-up of signals in the germanium detector. (XBL 8211-7470)

junction of 0.75 cm diameter surrounded by a silicon guard ring on the same wafer of 2.2 cm outer diameter. The center region is the active detector whose charge is collected by the dE/dx preamplifier, and after suitable pulse processing is digitized and stored as an LET value. The guard ring fulfills two functions: it defines the active central region wih high accuracy and it provides signals that can be used to veto a detected particle event if two or more particles would arrive at the germanium residual energy detector too close in time to be unambiguously separated by the pulse processing electronics.

The average energy deposited in the thickness of the LET detector can be calculated by the standard Bethe stopping power formula[17]:

$$-dE/dx = (4\pi z^2 e^4/mc^2\beta^2)NZ\{\ln[2mc^2\beta^2/I(1-\beta^2)]-\beta^2 + \text{correction terms}\} \quad (3)$$

where: z = the charge of the incident particle;

NZ = the number of electrons per unit volume in the medium;

β = the velocity of the incident particle in units of the velocity of light, c;

I = the mean excitation potential of the medium;

e = the electronic charge;

The Bethe formula is generally understood to be correct to within 2 or 3%. This sets the limit of accuracy in our LET calibration procedure.

The energy deposited by a charged particle in a thin detector follows a probability distribution given by the well known Vavilov distribution.[18] In addition, electronic noise in the detector system, a spread in particle

incidence angles, range straggling in absorbers, and the presence of fragments with the same atomic number Z as the primary particles (but with deficiency of one or more neutrons), can broaden the measured primary spectrum. In the measurements reported here, the electronic noise contribution is negligible and the other effects will dominate the width of the observed spectra.

Figures 4a,b, and c show LET spectra obtained by the silicon detector for a Ne-20 beam with a residual range of 32.3 cm in water after passing through a thin Pb upstream scatterer (0.08 cm), several foils in the beam line for monitoring equipment, 1.25 cm thick plastic walls of the variable water column (WC) and 0, 13.61 and 31.9 cm of water absorber, respectively. The primary peaks appear prominently at the right of the figures.

Figure 4a shows some particles with lower LET than the primaries. They have been generated by fragmentation in the various absorbers indicated above. In Figure 4b distinct peaks caused principally by fragmentation in the water absorber are observable. Peaks corresponding to fragments down to Z=5 are separable. For Z=4 and below, the peaks have coalesced in this simple histogram. The Vavilov distribution has a high energy tail that is most prominent when the detector is relatively thin. For the present case with heavy ions, a 300 micrometer silicon detector in the plateau region of the Bragg curve is not too thin (parameter $\kappa = 2.5$)[18] that the distribution is nearly Gaussian, as in Figures 4a and b. The calculated full width at half maximum (FWHM) of the Vavilov distribution for the case of Figure 4b is 3.35 keV/μm of water, which is essentially the FWHM of the measured peak.

As the width of the water absorber is increased, the shape of the Vavilov distribution for the primary LET peak should become more Gaussian-like than that of Figure 4b, but for monoenergetic particles, the calculated FWHM of the distribution should remain nearly equal to that case. The experimental

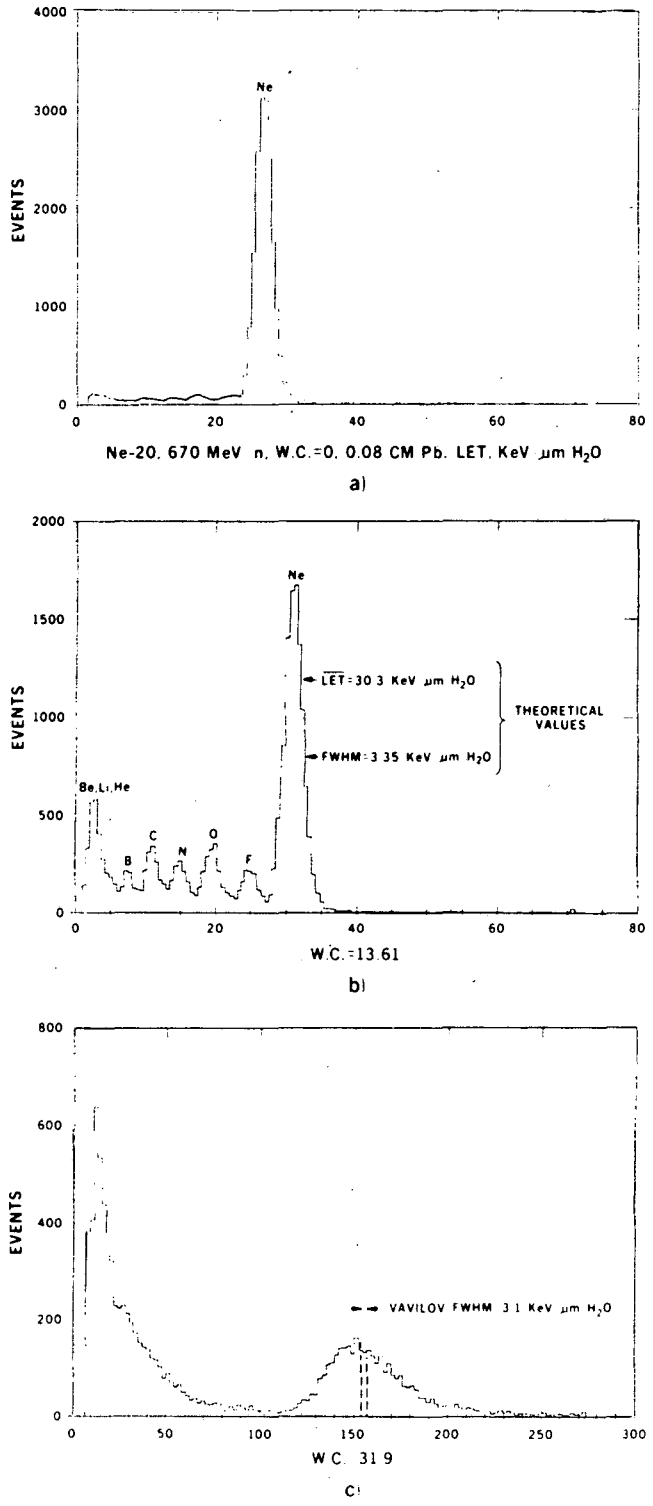

Figure 4
LET distributions for a 670 Ne-20 beam after passing through 0.08 cm Pb scatterer far upstream, several thin foils, and 1.25 cm plastic (water column walls). (a) water column = 0 cm. Some fragments are apparent in addition to the main LET peak from the primaries. (b) WC = 13.61 cm. Fragments from F to B are separated. Lighter fragments appear mixed in one single low LET peak. The primary peak, at 30.3 keV/μm, is found to follow the Landau-Vavilov distribution with the correct FWHM. (c) WC = 31.9 cm (residual range = 0.4 cm). The primary peak has been broadened considerably by range straggling and the presence of Ne-19 (long tail). The Vavilov value for FWHM of a mono-energetic beam is shown in the figure. (XBL 837-10786)

results, Figure 4c, show a primary peak that broadens considerably as the Bragg peak is approached, indicating the dominance of the range straggling effects, the presence of Ne-19 fragments, and possibly a wider spread in incidence angle of the particles. The theoretical FWHM of the corresponding Vavilov distribution for a monoenergetic beam is indicated in the figure. Because of the large number of low LET particles near the Bragg peak, the low LET cutoff for Figure 4c was set high (12.5 keV/μm water) in order to allow the display of the primary peak in a reasonable vertical scale.

The residual energy detector consists of two prisms of ultra high purity germanium forming p-n junctions of 1.5 x 1.5 cm cross section, and a total length of 5.5 centimeters or (18.7 cm water equivalent). The signals from both detectors are added at the preamplifier input, and the processed signal is proportional to the residual energy of a particle if it stops fully in the detector, or to the integral of the individual particle Bragg curve between the entrance and exit surfaces of the detector for those particles that do not stop in the germanium detectors. The proportionality between residual energy of a Ne-20 and the signal from a germanium detector has been demonstrated.[15]

Fragmentation of particles can occur in the detectors, with effects that are most important in the germanium detector. The lateral dimensions of the germanium detector were made twice the diameter of the central region of the dE/dx detector in an attempt to catch as many of the fragments generated in the germanium detector as possible. Also, the beam composition near the Bragg peak may contain particles that travel at substantial angles with respect to the original beam direction. The larger germanium detector dimensions are intended to help identify those particles. For that same reason, the distance between the silicon and the germanium detectors has been kept as small as possible, approximately 0.5 cm.

III. ELECTRONICS AND SYSTEM CHARACTERISTICS

The signals from the dE/dx and E detectors are integrated by charge sensitive amplifiers and further processed by pseudo-Gaussian shaping amplifiers. An event is recorded whenever a particle arrives at the central region of the dE/dx detector and is not preceded or followed too closely by another particle in the same region or in the guard region of the same detector, thus avoiding an erroneous result due to pile-up in the silicon and/or the germanium detector channels. The two regions of the silicon detector are also used together to count all the particles that deposit energy above a certain threshold. We call that function of the silicon detector the downstream counter (DC).

A calculation of the energy that a single fast proton would leave in the LET detector, and that of a heavy ion near the Bragg peak, indicates that the dynamic range of the measurement attempted is of the order of 1:2000. The operation of readily available event discriminator circuits at dynamic ranges larger than approximately 1:200 has not been possible. For that reason, the measurements reported in this paper have been carried out with event discriminators set at the relatively high LET values of approximately 1.0 keV/μm of water. The effect of the discriminator settings is to neglect very low LET particles in the analysis. They appear to have a strong contribution to the number of particles found at regions near and past the Bragg peak, but only represents a small contribution to the dose. Discriminator circuits are now under development at the Lawrence Berkeley Laboratory which will allow us to correct in great part the above deficiency.

The pile-up rejection circuit considers any events occurring within 300 nsec as a single event. The width of this time interval is determined by the characteristics of amplifiers needed to implement large dynamic range event

discriminations, as discussed above. Experiments are carried out at particle fluences sufficiently low (10^4 particles per cm^2 per beam pulse lasting approximately 0.6 seconds) to make it highly unlikely that two primary particles will deposit energy in the central region of the silicon detector within such a short time. When a primary particle fragments in an absorber prior to arriving at the detector, however, all the fragments that move forward in a tight cone may strike the detector within that time interval and will, therefore, be recorded as one event. If the fragmentation consists of one high Z particle and one or several low Z particles, the resulting detected event will be, in all appearances, one with the single high Z particle because LET is proportional to Z^2. The existence of the low Z particles then results in some broadening of the obtained spectra. The sum of the LET values of all the particles in a cluster is recorded, although their individual contribution cannot be established. In order to avoid this ambiguity, subnanosecond measurement capabilities are required as in Reference 14 which uses time-of-flight methods. Our requirement for simplicity and portability precludes the use of such techniques.

Particle events that pass the timing tests described above are accepted, digitized, and stored in a 33 megaword disk through a CAMAC interface on a PDP 11/34 computer. Pulse processing time for the signals is approximately 2 μsec for the detector electronics, 80 μsec for digitizing, and approximately 35 μsec for read and storage operations. A maximum acquisition rate of approximately 32,000 words per second was demonstrated for the computer data acquisition system, grouping six words per event. The relatively slow speed of the digitizing operation is a reasonable match for the read, transfer, and storage characteristics of the computer and disk system.

During data acquisition, or off-line at a later time, the data stream is analyzed by the PDP 11/34 computer with the assistance of a fast array processor. A two-dimensional histogram of dE/dx vs E is generated with data that meet a certain number of criteria, e.g., minimum and/or maximum energy in any of the variables, data that belong to a specific beam pulse of the Bevalac. The processor completes the tests and histograms of 20,000 events in a few seconds. The histogram is displayed in a 128 x 128 color or b/w video display. Analysis programs then take over the task of identifying the particles corresponding to each element of atomic number Z in the two-dimensional histogram and to carry out desired calculations.

IV. TWO-DIMENSIONAL DATA ANLAYSIS

The technique of particle identification from the time-coincident dE/dx and E signals was used with heavy-ion beams of biomedical interest at the Lawrence Berkeley Laboratory by Maccabee[19] and Maccabee and Ritter[20]. Goulding and Harvey[21] reviewed the field of particle identification, and contributed important algorithms and circuits to the art. Schimmerling and Curtis[22] made time-of-flight measurements with 3.5 GeV nitrogen ions. Schimmerling et al,[14] used an identification algorithm developed by Greiner[23] based on a least-squares method. There is, in addition, a large number of examples in the literature of the use of dE/dx vs. E and time-of-flight information for particle identification.

We have encountered substantial problems, however, in attempting to analyze our data by methods that are usually intended for particle identification after thin absorbers. In the interest of data analysis speed, we have also rejected particle-by-particle analysis methods, and have

concentrated our effort in analysis methods that could work globally on a two-dimensional hystogram of all the data acquired.

The most valuable option we have found is based on a calculation of the loci of dE/dx vs. E for the different particles that can be found as a result of an experiment from first principles, from the detector calibration parameters, and the known thickness of the detectors. With very minor corrections to the calibration parameters, we invariably find that the detected particles cluster around the calculated loci.

Figure 5a shows a two-dimensional histogram of dE/dx (or LET) vs. E for a Ne-20 beam with a residual range of 1.4 cm after passing through a water column of 31.9 cm. Figure 5b shows the calculated loci overlaying the experimental results. Fragments that appear at the high E side (right) in a particular locus are those that are generated in the upstream side of the absorber, while those appearing towards the low E side have been generated nearer the detector. The analysis procedure assigns every cell of the two-dimensional histogram to a particular value of Z depending on its distance to the individual calculated loci. In this manner the components of a beam can be rapidly separated automatically and individual two-dimensional histograms corresponding to each value of Z can be obtained for further analysis.

Fragmentation of particles with high residual energy in the long germanium detector presents only minor difficulties in the analysis, since the particles leave their correct value of LET in the silicon detector and their identification is not complicated by the curved loci of the low residual energy particles. Figure 6 shows a two-dimensional histogram for the same Ne-20 beam as in Figure 5, but with a total of approximately 1.5 cm water equivalent absorber only. Particles along the horizontal line are the result of

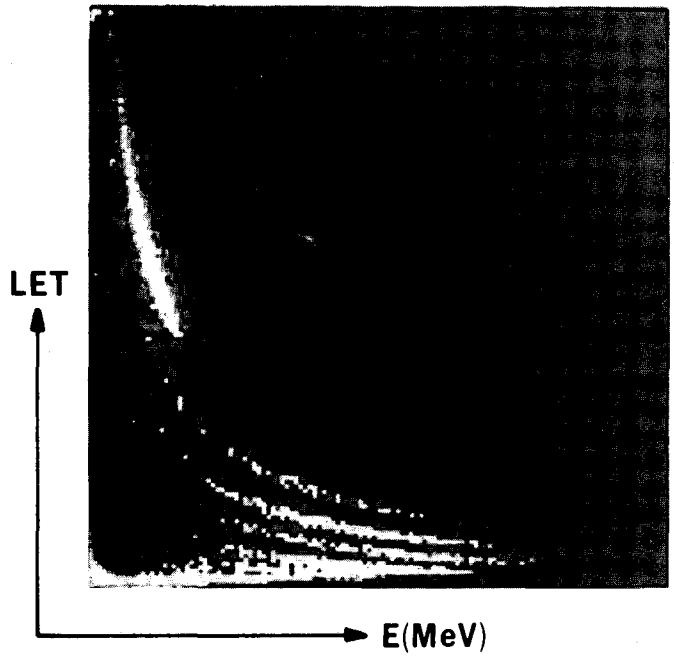

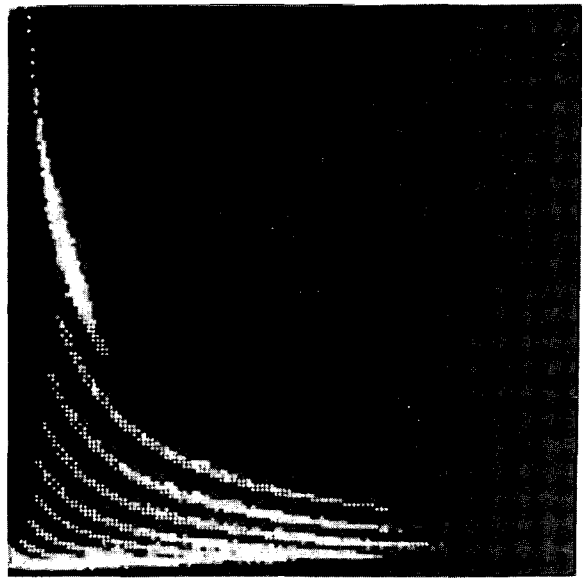

Figure 5
(a) Two-dimensional histogram of LET (ordinate) vs. residual energy (abcissa) for a 670 MeV/n (Bevatron extraction energy) Ne-20 beam, after passing through a 0.08 cm. Pb scattering foil far upstream, and a 31.9 cm water absorber. The lighter locus at the top left corresponds to the surviving primaries, with each gray line corresponding to fragments of decreasing atomic number by 1. At bottom left one can observe numerous light fragments. Brighter pixels correspond to higher number of particles of the corresponding LET and residual energy. (b) Theoretical loci corresponding to the various values of Z calculated form first principles and the detector calibration parameters superimposed on experimental results. Only minor adjustments (a few percent) are needed to secure the fit between theory and experiment. The theoretical loci are used in assigning pixels in the histogram to specific values of Z for analysis. (XBB 837-6241A)

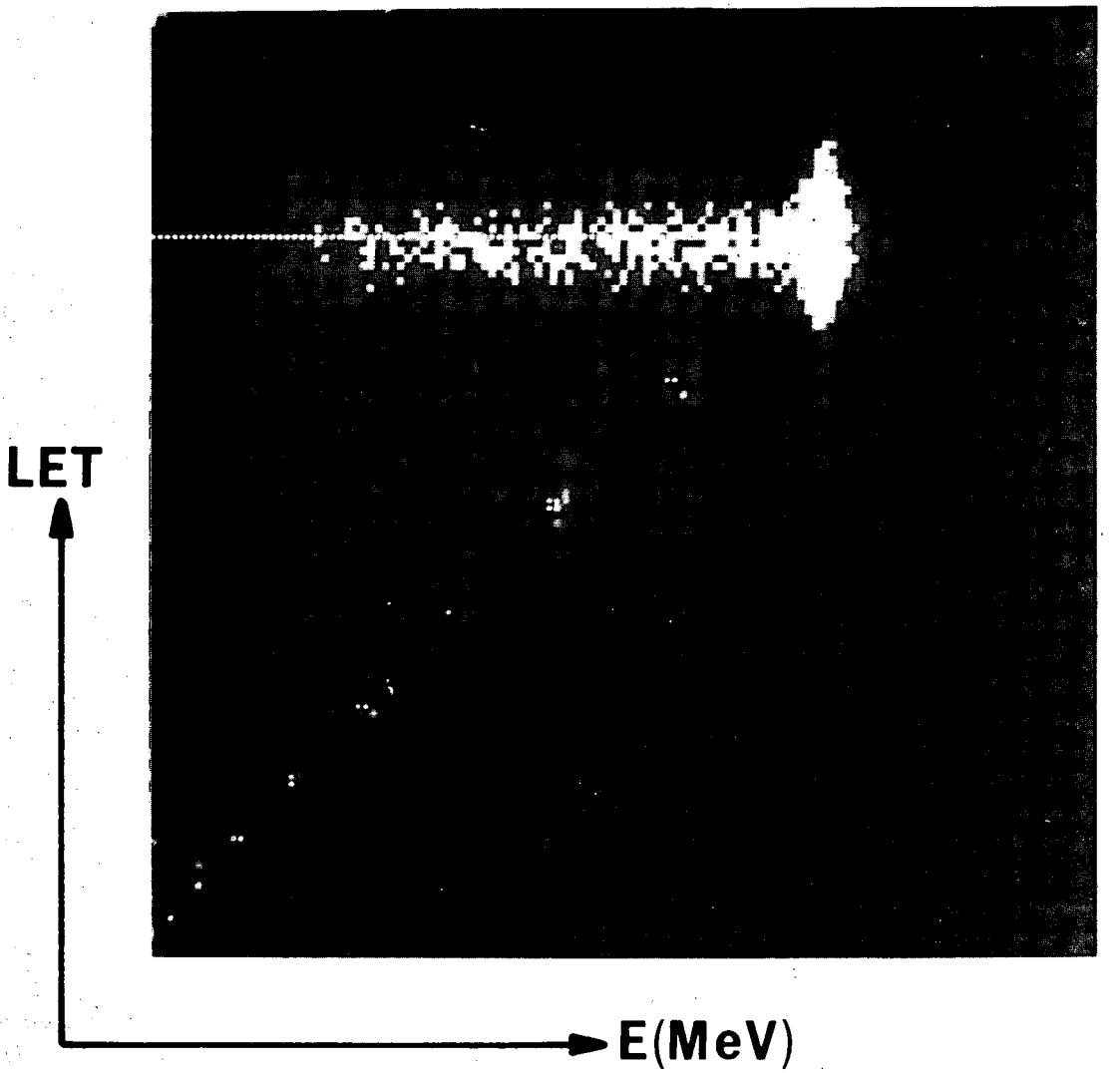

Figure 6
Two-dimensional histogram with superimposed theoretical loci (points or lines) for the same 670 Ne-20 beam of Figure 3, but with 1.5 cm water absorber. The bright large spot corresponds to unfragmented primaries not stopping in the thick germanium detector. The "tail" to the left is due to fragmentation in the germanium detector. (XBB 837-6243A)

fragmentation in the germanium detector, but are unambiguously identified as primary neon.

Particles of identical Z, but different A cannot be separated in our measurement. The statistical fluctuations in the energy deposited by the particles in the detectors (Vavilov distribution) are of sufficient magnitude to make that fine distinction impossible.

The water equivalent length of the germanium detector is not sufficient to stop all the particles in many cases. The loci of dE/dx vs. E then do not consist of simple curves, but they exhibit folding into the locus of a neighbouring Z, as in the case of Figure 5 for Z=6 and below. When this effect occurs, it is not possible to assign particles to the different values of Z unambiguously. For that reason the data presented in this paper for low Z particles are usually presented in groups. This is a necessary limitation of the simplicity of the detector system. It could be corrected, in part, by making a longer germanium detector.

V. MEASUREMENT OF INDIVIDUAL PARTICLE LET

The first measurements of average LET (track average) to be reported here correspond to Ne-20 and Si-28 beams of 670 Mev/nucleon nominal energy (Bevalac extraction energy), in standard irradiation setups. The Bragg curves measured for the central 1 cm diameter region of the beams by ionization chambers are shown by solid lines in Figures 7a and 7b. The thickness of the upstream Pb scatterers was 0.32 and 0.27 cm, respectively. The depths of the water column for which measurements are reported appear as solid circles in the same figures.

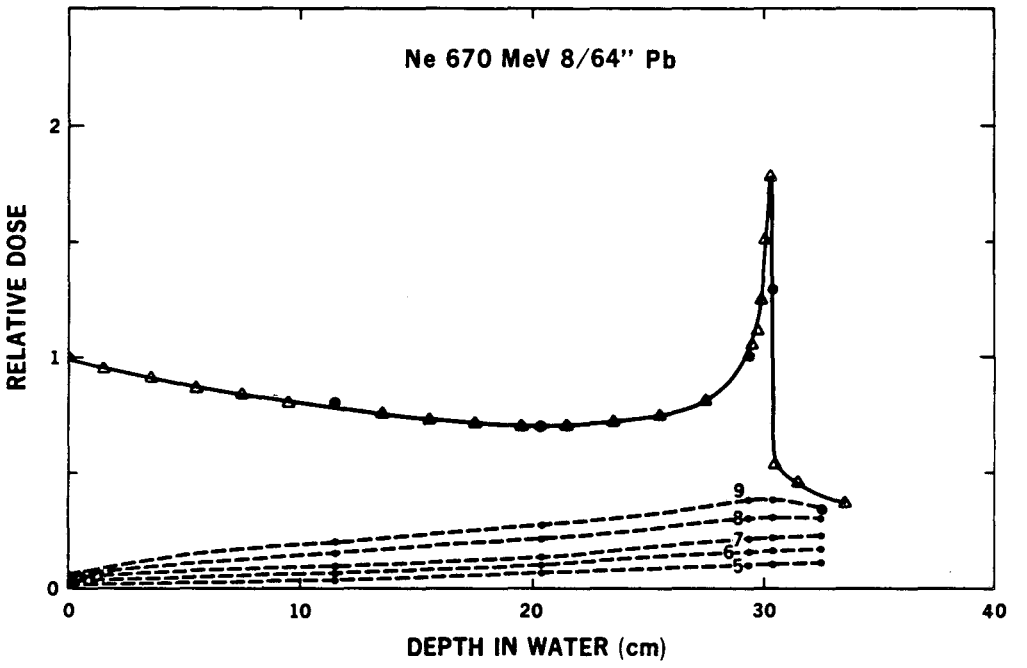

a)

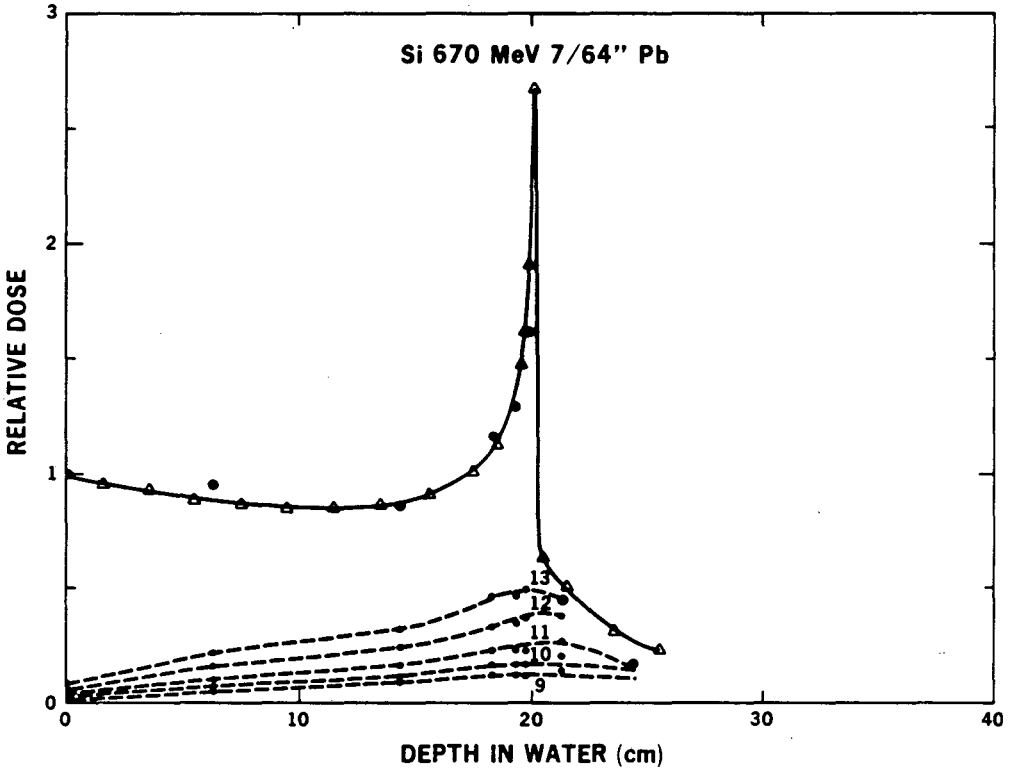

b)

Figure 7
(a) Bragg curves for a 670 Ne-20 beam, after passing through 0.32 cm Pb scatterer far upstream. The solid line corresponds to values obtained by ionization chambers. The solid dots (•) correspond to the points obtained from the data reported in this paper. Curves labelled 5 to 9 correspond to cumulative dose distributions for fragments from the lowest Z detected to the given Z. Thus, curve 9 corresponds to dose contribution by all fragments. (b) Bragg curves for a 670 Si-28 beam, after passing through 0.27 cm Pb scatterer far upstream. The eight measurement points are indicated. Z = 13 curve corresponds to dose delivered by all fragments. (XBL 837-10785)

Average LET for individual values of Z has been calculated from projections onto the vertical axis of two-dimensional spectra like those of Figures 5 and 6 in which the individual components have previously been separated. The quantity measured directly is energy deposited in the silicon detector, which is converted to stopping power by dividing by the detector thickness. The stopping power in water is obtained from that in silicon by dividing by 1.95, a factor that remains essentially constant at all the energies of interest. The fitting of the experimental results in two-dimensions at different water column absorber settings by the theoretical particle loci for component separation has sometimes required small adjustments (typically 2 to 5%) in the calibration factors of the detector electronics, as indicated above.

Figures 8a and 8b show the calculated values of average LET in water for the primary particles Ne-20 and Si-28 (solid lines) obtained from Equation 1. The experimental track averages for the same primaries at different water absorber settings used are also shown. The agreement implies that within the small corrections that we sometimes apply to the calibration factors, the measurements agree with theory.

Figure 8a also shows the measured track average LET for individual fragments with atomic numbers 6 to 9. LET values for fragments with values of $Z<5$ have been grouped into one single curve because the individual components are difficult to separate. Figure 8b shows similar results for the Si-28 measurements. Average LET for fragments with $Z=9$ have been presented in a one curve.

An estimate of the statistical errors in the measurement of average LET has been done in a simplified manner by noting that the individual particle LET spectra at different points of the Bragg curve is roughly Gaussian, with the

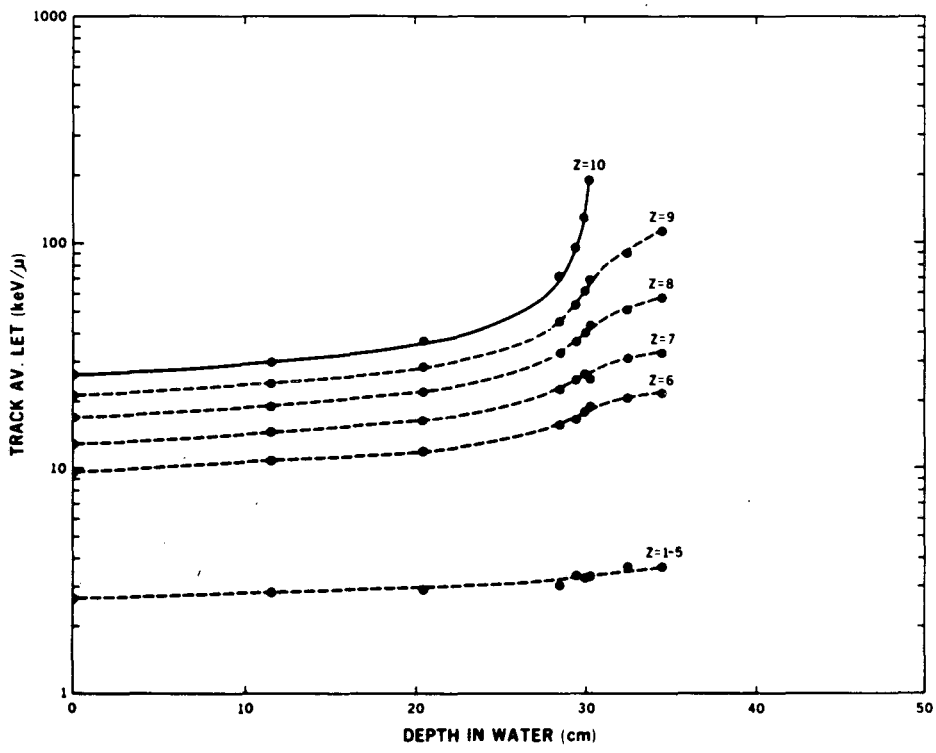

a)

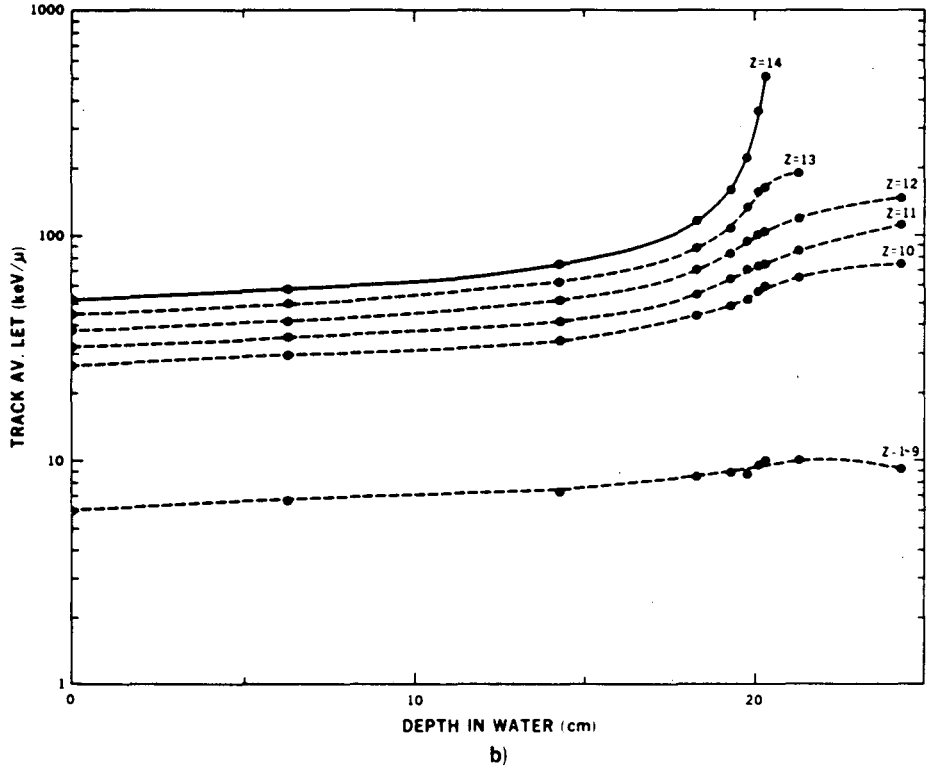

b)

Figure 8
(a) Measured track averaged LET for particles of different Z for the 670 Ne-20 beam. Particles with Z = 1 through 5 have been given as a single curve due to difficulty in separation of the various Z components. The electronics system did not respond to individual fast protons. The solid line corresponds to the LET calculated from the Bethe stopping power formula. The agreement with experimental results has been obtained by making occasional small corrections to the calibration factors of the LET detector. (b) Measured track average LET for particles in a 670 Si-28 beam. Particles with Z=1 to 9 have been grouped into one single line. See text for estimation of errors. (XBL 837-10787)

largest departures at points near the Bragg peak. For a sampled Gaussian distribution in which the number of counts in each sample bin is Poisson distributed (our case), determination of the centroid by the simple method of finding the first moment and dividing by the number of particles yields a standard error which is proportional to the standard deviation of the Gaussian shape divided by the square root of the total number of counts in the Gaussian. The proportionality constant is dependent on the actual shape, but can be expected to be near unity[24].

With the number of particles accepted at each point of the experiments (10,000 or 20,000), we find that the largest standard errors in the values plotted for individual values of Z in Figures 8a and 8b are approximately 1 keV/μm, which correspond to the case of the very broad distribution in LET of Z=13 particles (Al) in the Si-28 beam near the Bragg peak. This corresponds to less than 1% standard error in that particular case. At most other points the statistical errors are substantially smaller. For that reason, no error bars have been included in Figures 8a and 8b; forcing the average primary LET to fit the results of Equation 1 can result in errors of ± 2 or 3% at any point in the graphs.

VI. MEASUREMENT OF BEAM COMPOSITION

The determination of the numbers of particles of each individual atomic number existing in a complex beam has been approached in two steps:

(1) Finding the probability that a primary particle being delivered by the accelerator will arrive at the LET detector in any form (as an unfragmented primary, as a single secondary, or as a cluster of secondaries), and

(2) finding an unbiased probability distribution that a detected particle will

consist of an ion of atomic number Z (which could be accompanied by lighter ions, as discussed above).

The first probability, which we call transmission, T, is obtained by dividing the number of counts in the downstream counter (DC) by the number of counts in the upstream counter (UC). When normalized by the ratio obtained at zero water absorber, the values of T for a given beam delivery configuration are an indication of the appearance or disappearance of particles in the area covered by the LET detector as the amount of absorber is increased. The DC functions at high speed, undeterred by the digitizing time of ADCs or computer storage delays.

The second probability is obtained from the dE/dx vs. E histograms. Since the data acquisition system requires the same amount of time to process an event, regardless of the magnitude of any parameters, the two-dimensional histogram is unbiased, i.e., the probability of an event being recognized by the computer system for digitization is independent of the magnitude of the parameters of the previous event or of itself. After a two-dimensional histogram has been acquired and the different components separated by the analysis process described above, a division by the total number of events recorded yields the desired probability distribution, p(Z).

The product T x p(Z) is then the probability P(Z) that a primary ion being delivered by the accelerator arrives at the LET detector as an ion of atomic number Z or as an ion cluster with one of them having a high atomic number Z, the rest being of low atomic number. Again, we cannot distinguish between the two cases.

Special care has to be taken in measurements of T with a guard ring silicon detector. If one were to use only the center region of the detector as DC, large signals in the guard region will result in a small signal fed to the

center region through the capacitance between the two regions. That signal will trigger the counter, resulting in erroneous values of T (too high) at regions near the Bragg peak (where signals from primaries are large). We use the two regions of the silicon detector together to avoid the problem. Also, the discriminator settings for the DC have to be low enough so that, as we approach the Bragg peak, the observed large number of light fragments is properly recorded by the DC. Otherwise, too low values of T are obtained. With the approximately 1 keV/μm setting of the discriminator, we have been able to measure T and p(z) sufficiently well to reconstruct the Bragg curves for neon and silicon beams with reasonable accuracy. T remains close to unity until the vicinity of the Bragg peak, where it starts dropping. Figures 7a and 7b show with solid circles the Bragg curve points reconstructed from our data. We are probably still missing a substantial number of low LET particles, as the reconstructed points past the Bragg peak are somewhat low.

Figures 9a and 9b show the probabilities P(Z) that a primary delivered by the Bevatron reaches the LET detector as a particle of atomic number Z. P(Z) for the primaries is less than unity at 0 cm absorber because of the presence of upstream lead absorber, water column windows, and ion chambers in the beam line. The data presented for each value of Z, including the primary particles, include the isotope with one neutron less than the stable isotope of the same Z. The primaries exhibit a mean free path of 19.83 cm for the Ne and 15.50 cm for silicon. It is interesting to compare this value with other experimental and theoretical results. Lindstrom et al.[25] measured absorption cross sections σ for C-12, O-16 and Ar-40 beams at near 2 GeV/n for a number of targets between H and U. They found that σ can be expressed as:

$$\sigma = \pi r_0^2 \left(A_B^{1/3} + A_T^{1/3} - b^2\right) \qquad (4)$$

with errors less than 10% for all the particles studied, where $A_{B,T}$ are the atomic numbers of the beams and target particles, b is an overlap parameter which depends on the particles, and $r_0 = 1.29 \times 10^{-13}$ cm. The cross sections obtained from equation (4) are in excellent agreement with the theoretical calculations of Townsend et al.[26] at 2 GeV. For the range of energies of our measurements, the theory predicts a decrease in cross sections of approximately 20% for a Ne-20 beam and 10% for A-27 (close to Si-28). With those corrections, the predicted mean free paths for our beams are 18.55 cm and 14.35, respectively, which are reasonably close to our measurements. The differences could be due to the inclusion of Ne-19 and Si-27 fragments with the primary particles.

Individual values of P(Z) are also shown in Figure 9a for values of Z from 6 to 9. The separation of particles below Z=6 cannot be carried out with accuracy. We present, therefore, one curve indicating P(Z) for atomic numbers of 5 and below. The large number of particles in that curve is due principally to the lightest measurable fragments.

Figure 9b shows corresponding results of P(Z) for the silicon primary beam. Individual curves for Z = 10 to 13 are shown, as well as one curve for Z < 9. The low energy threshold of the measurement was not low enough to detect individual protons.

The calculation of statistical errors in the particle numbers follows in a straightforward manner from considerations relative to Monte Carlo methods.[27] A measured probability P(Z) that a primary particle ends up with a particular value of Z will be correct to $\pm\,\varepsilon$ with 95% confidence when:

$$\varepsilon = 2/\sqrt{[N/P(1-P)]} \qquad (5)$$

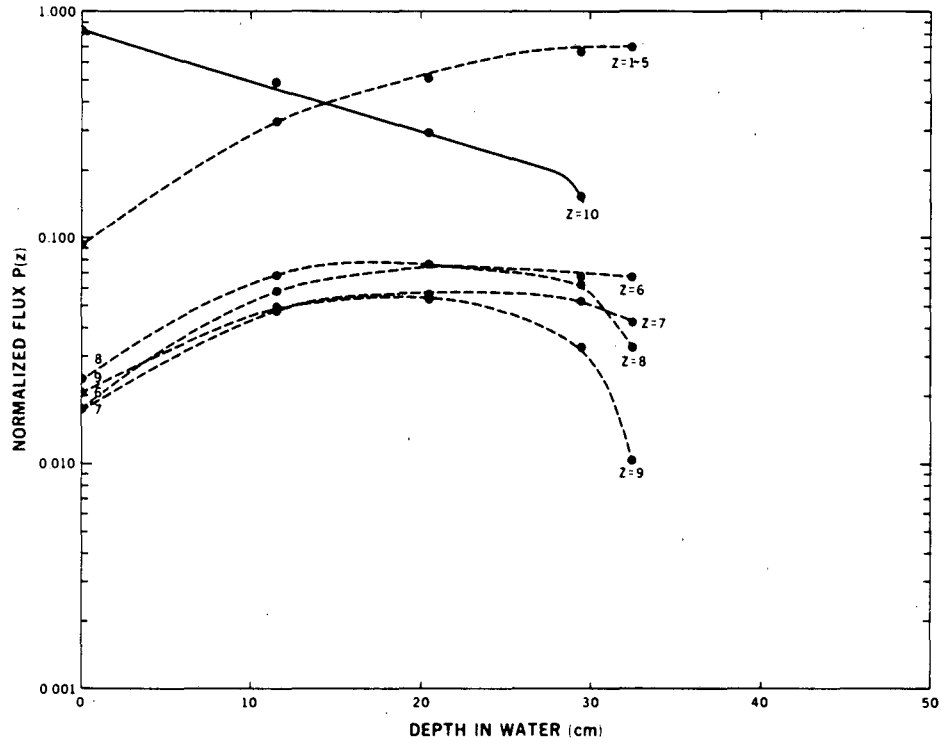

a)

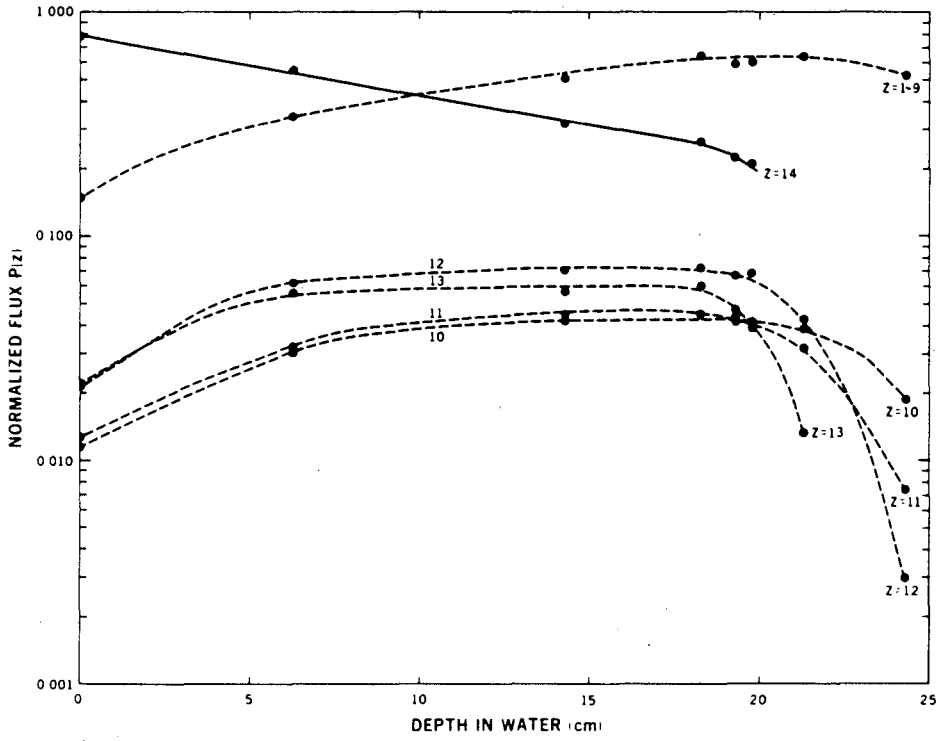

b)

Figure 9
(a) Particle flux P(Z) measured for the Ne-670 beam. It corresponds to the probability that a primary delivered upstream of any absorbers reaches the detector system with a particular value of Z. A heavy fragment may be accompanied by some lighter particles that cannot be separated by the detector system. Note that at zero water depth, the beam has traversed a lead absorber, two or three ionization chambers, several metal windows and approximately 1.25 cm of plastic for the walls of the variable water column. For that reason, P(10) at zero water is not unity. (b) The same is true for the 670 Si-28 beam; seee text for estimation of errors. (XBL 837-10788)

where N = total number of primary particles measured, and P is approximated by M/N, M being the number of primaries found to have fragmented to the given Z. Error bars corresponding to 95% confidence in the values of Figures 9a and b would extend to approximately ± 10% of the plotted results for all individual secondary curves, to approximately ± 5% for primaries and to approximately ± 1% for the low Z groups.

VII. FRACTION OF DOSE DUE TO FRAGMENTS

The two-dimensional histograms of dE/dx vs. E obtained at different points in the Bragg curve of a heavy ion beam contain all the information needed to calculate a number of parameters of interest to radiobiologists and therapists. The simplest cases correspond to calculations of track and dose average LETs of the complete beam, of individual components or of groups of components. During the process of breaking down a two-dimensional histogram into its components of different Z, the data processing programs calculate the first and second moments of the LET histograms for each value of Z.

Track average LET for a group of particles with values of Z from Z_i to Z_j is calculated from:

$$LET_t = \sum_{Z_k=Z_i}^{Z_j} \frac{(\sum_n N_n \times LET_n)_{Z_k}}{(\sum_n N_n)_{Z_k}} \qquad (6)$$

where N_n is the number of particles in one bin for the LET histogram of particles Z_k, LET_n is the LET of that bin, and the summation over n is over all the bins in the histogram.

The dose average LET is obtained from:

$$LET_d = \sum_{Z_k = Z_i}^{Z_i} \frac{\left(\sum_n N_n \times (LET_n)^2\right)_{Zk}}{\left(\sum_n N_n \times LET_n\right)_{Zk}} \qquad (7)$$

As an example of a whole beam LET and dose distribution, Figure 10a shows the LET distribution for the 670 Mev/nucleon Si-28 beam at a residual range of 1 cm. The large number of very low LET particles results in a graph in which the primaries and high Z secondaries appear very depressed. Figure 10b shows the corresponding dose histogram (number of particles in a channel x its LET, i.e., the first moment). The contribution of the primaries is now quite prominent. The integral of the dose distribution is also shown. Approximtely 64% of the dose is delivered by the primary particles at that point in the Bragg curve.

The cumulative dose contribution by particles up to and including a certain value of Z is shown in Figures 7a and b. The curve for Z=9 in the case of Ne-20 and that for Z=13 in Si-28 correspond to the fraction of dose delivered by all measured fragments. The shape of the fragment dose contribution agrees reasonably well with the calculations of Lyman (Ref. 4), as well as the observation that at the Bragg peak position, the fraction of dose due to secondaries is 40 to 45% of the total dose. (Lyman's calculations were for a 557 MeV/nucleon Ne-20 beam, which is approximately equivalent to our 670 Mev extraction energy beam.)

Finally, Figures 11a and b show track and dose average LETs for the complete beams of Ne-20 and Si-28 described in this paper. The values of track averaged LET, obtained from the two-dimensional histograms alone, follow very closely the Bragg curves of Figures 7, which is expected with values of T near unity. The estimates of errors in Figure 11, shown only for the dose averaged

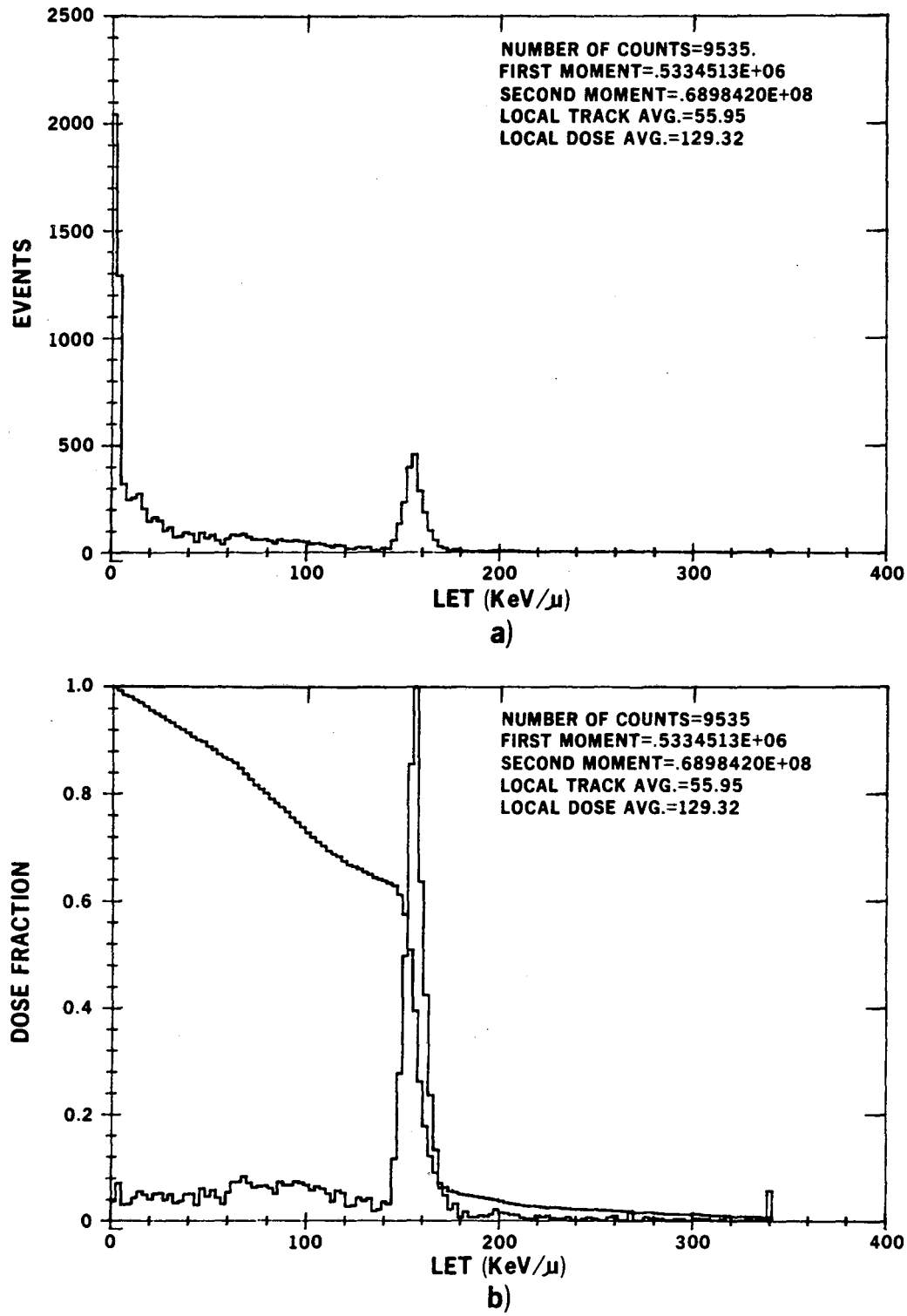

Figure 10
(a) LET distribution for the 670 Si-28 beam at a residual range of 1 cm. Notice the large number of light fragments in the beam. (b) Dose distribution for the same Si-28 beam at 1 cm residual range, obtained by multiplying the number of particles in a particular bin of the LET distribution by the LET and normalizing. An integral of the dose distribution is also shown, indicating approximately 64% of the dose is delivered by primaries with LET greater than 140 keV/μm. (XBL 10784)

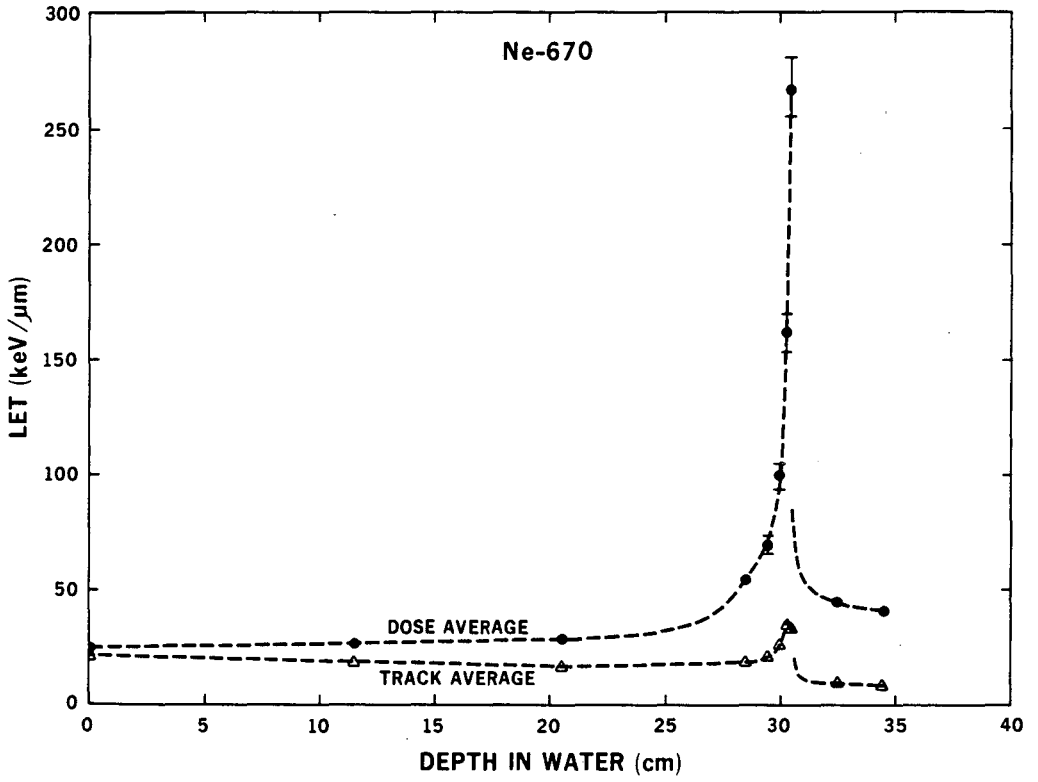

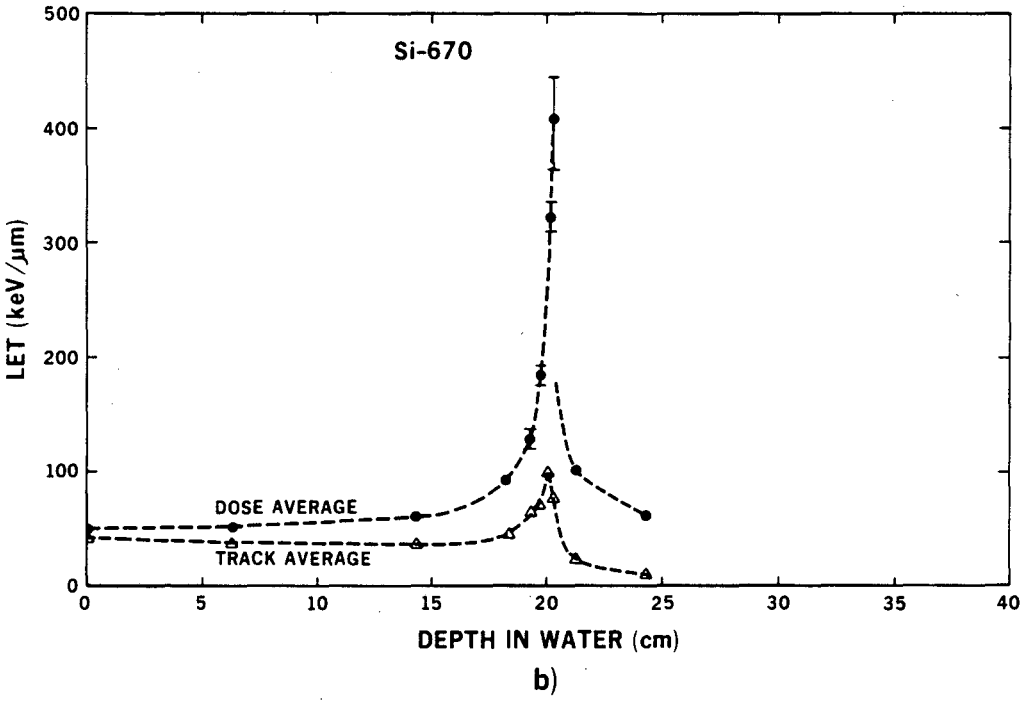

XBL 837-10783

Figure 11
(a) Track and dose-averaged LETs as a function of depth in water for the 670 Ne-20 beam, and (b) for the 670 Si-28 beam. (XBL 837-10783)

LETs at 95% confidence level, have been obtained principally from the statistical errors in the numbers of primaries.

VIII. VELOCITY DISTRIBUTIONS

One of the ideas that shows promise in understanding and predicting the inactivation of cells by high LET radiation[3] is based on the assumption that particle track structure is one of the important characteristics defining the behavior of a beam. Three variables for each component of a beam are then required to describe it: fluence, particle velocity and charge.

Fluence and charge can be obtained for a beam analyzed by the methods described above. Particle velocity is not measured directly by our detector assembly, but an approximate value of velocity can be calculated for particles that stop in the germanium detector. If we assume that the mass number A of a fragment characterized by a particular atomic number Z is only the one for the stable isotope, we can rescale the individual histograms for each value of Z obtained from the two-dimensional histogram of dE/dx vs. E (total kinetic energy) by making individual plots of dE/dx vs. E' (in Mev/nucleon) and then adding them. In the new histogram, particles in a vertical column have the same velocity, which can be calculated from:

$$\beta^2 = \frac{[1 + (E'/931)]^2 - 1}{[1 + (E'/931)]^2} \qquad (8)$$

Figure 12a shows a two-dimensional histogram obtained from the 670 Mev/n Ne-20 beam described above, at a residual range of 0.9 cm. The primary particles and secondaries down to Z=6 appear to stop fully in the germanium detector, although there is some question about the Z=6 case. A rescaling for particles between Z=6 and 10 is shown in Figure 12b. The abcissa is now

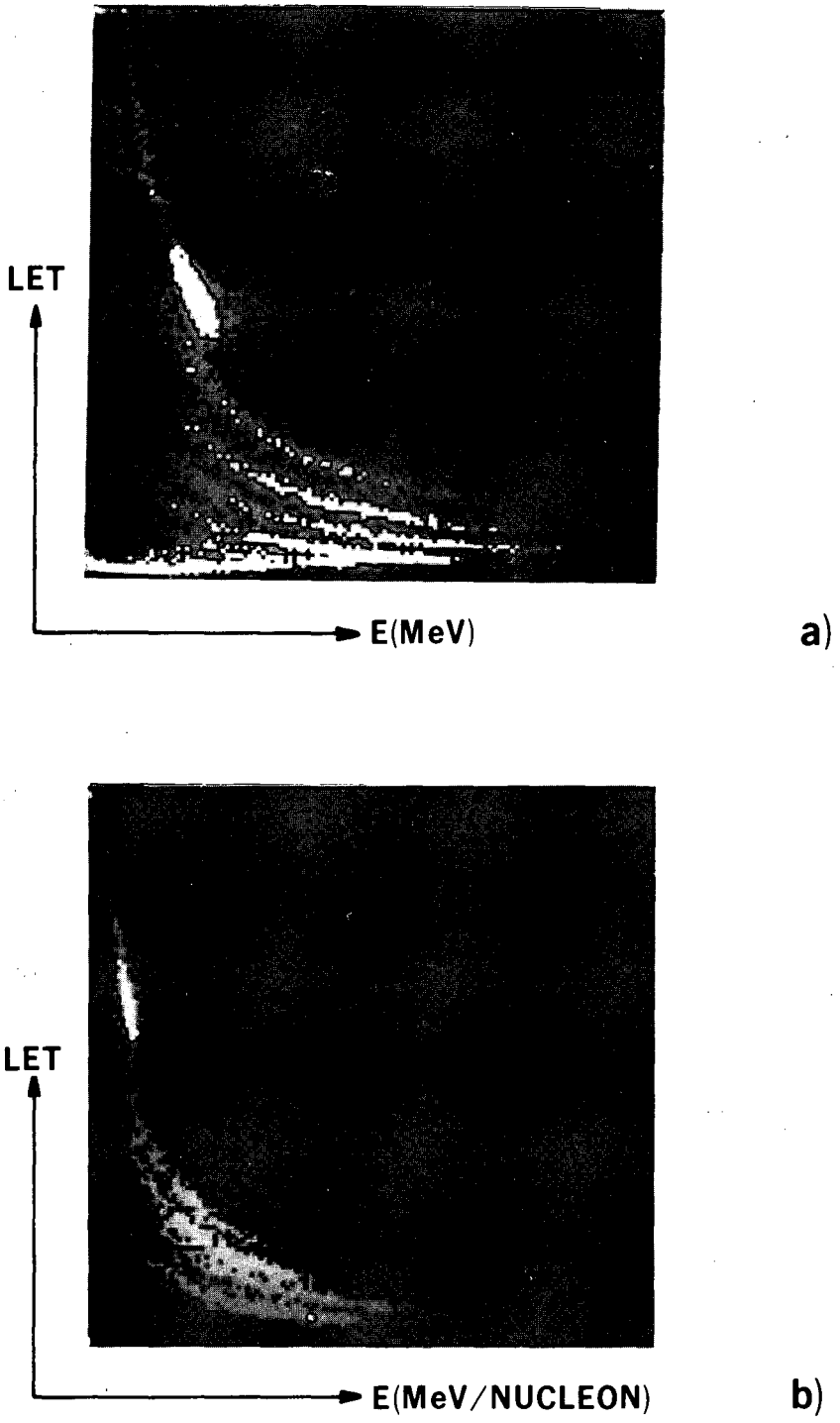

Figure 12
(a) Two-dimensional histogram of LET vs. residual energy for a 670 Ne-20 beam after passing through 0.08 cm Pb scatterer, at a residual range of 0.8 cm. (b) Two-dimensional histogram of LET vs. residual energy in MeV/nucleon replotted from Figure 12a from the separated components for Z = 6 to 10. Particles corresponding to the same residual energy in the new histogram have the same velocity. There are no fragments slower than the primary peak, as expected from the assumption that all fragments are generated with the same velocity of the parent particle at the point of fragmentation. (XBB 837-6240A)

presented in MeV/nucleon. There are no fragments that are slower than the surviving primary particles, as one would expect if fragmentation events create secondaries with the same velocity as the primary at the point of collision.

Figure 13a shows the distribution of primary particles as a function of energy in MeV/nucleon. Figure 13b shows the corresponding distribution for Z=9. Note the sharp cutoff at the low energy end, coinciding with the low energy cutoff of the primaries. Figure 13c shows the distribution Z=8, with a shape that is characterisitic of intermediate values of Z; Figure 13d shows the distribution for Z=6. The sharp cutoff at the higher energy end is caused by the finite length of the germanium detector. Carbon particles generated far upstream do not stop in the detector. The missing part of the spectrum is actually folded up about the high energy cut off.

It is interesting to note that the lowest value of Z for which velocity can be calculated depends only on initial energy and depth of the water absorber. For 670 MeV/n, near the Bragg peak, Z=6 is the limit, both for a Ne-20 and a Si-28 beam. Clearly as we lower the atomic number of the fragment, the first ion that will not stop fully in the residual energy detector will be an ion generated far upstream in the absorber, regardless of how many nucleons the primary ion had to loose in order to generate it.

IX. CONCLUSION

The development of the simple two-detector system described in this paper opens the possibility of measuring rapidly and with useful accuracy a number of beam parameters which are of importance to radiobiologists and therapists. The LET measurements, particle identification, dose calculations, and the determination of velocity distributions will be useful in studies of radiobiological efficiency and oxygen enhancement ratio of heavy ion beams,

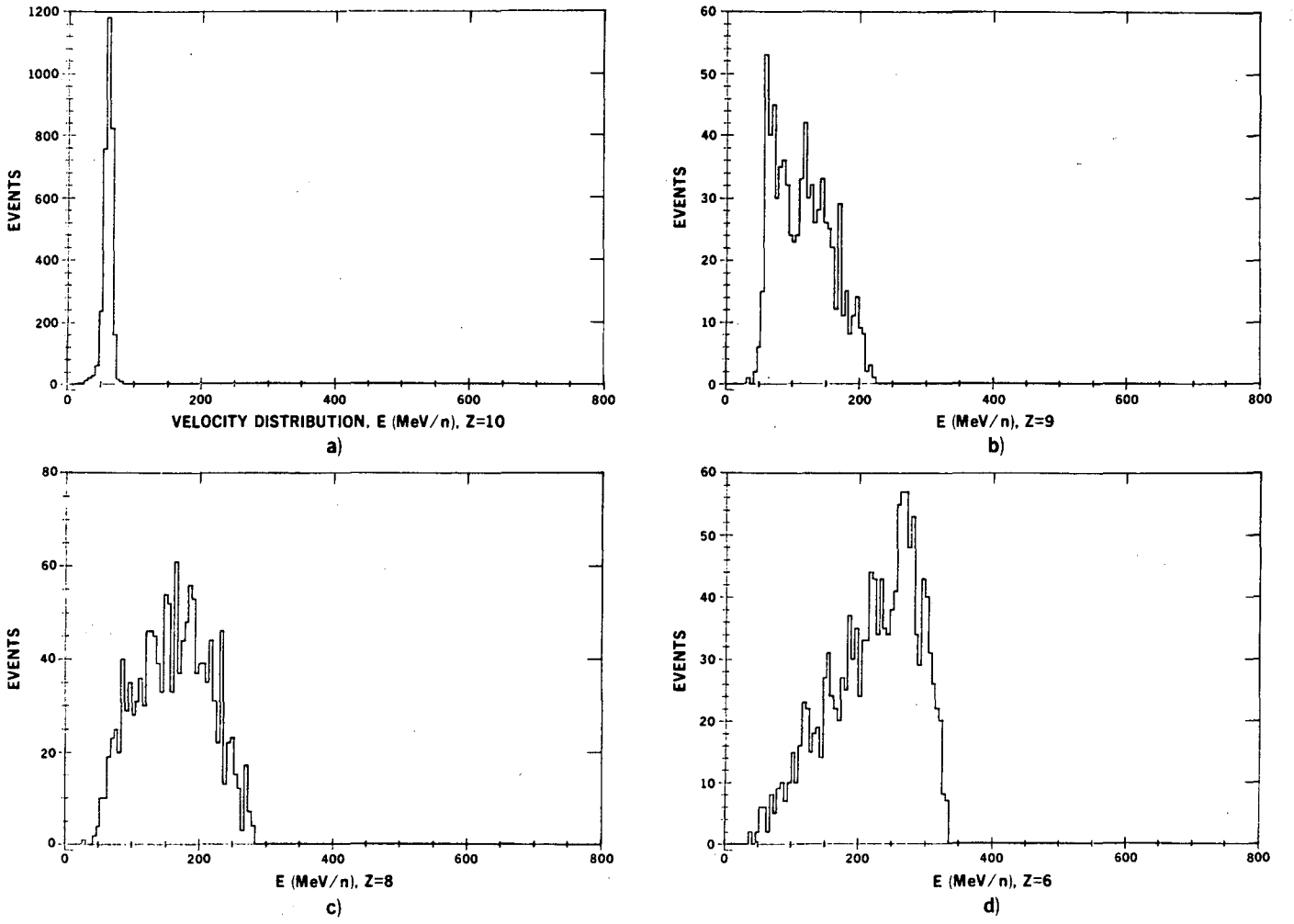

Figure 13
(a) Residual energy distribution in MeV/nucleon for primary particles of Figure 12. The abcissa is related to velocity by Equation 4. Identical values of residual energy in Mev/n correspond to equal velocity, independent of atomic number. (b) Repeat of Figure 13a only for Z = 9. Notice the sharp low velocity cut-off, coinciding with that of the primary particles. (c) Repeat of Figure 13a only for Z = 8. This is a Gaussian looking shape typical of particles with intermediate Z. (d) Repeat of 13a only for Z = 6. The finite length of the germanium detector results in an erroneous measurement of residual energy for the faster C particles in the beam, resulting in a folding of the spectrum over the sharp high energy cut-off. (XBL 837-10789)

supplementing previous theoretical calculations, and assisting in improving them, and in the assessment of the validity of various models for cell inactivation and mutation. The measurement technique will also be useful in absolute and comparative measurements of beam quality with new beam delivery systems at the Bevatron intended to minimize effects of fragmentation and beam nonuniformity, and for establishing the consistency of beam characteristics in day-to-day radiation therapy. Measurements of fragmentation in different kinds of tissues can also be undertaken. The detector system still needs more development before it can be used routinely: It will be important to increase the dynamic range of the event discriminators so that fragments lighter than the ones observed at present can be measured. We should be testing new circuits for that purpose in the near future.

ACKNOWLEDGEMENTS

The authors would like to acknowledge valuable discussions with A. Chatterjee, E. Blakely, S. Curtis and the members of the Beam Quality Group, Donner Laboratory, LBL. The authors are very thankful to F. Goulding, D. Iandis, N. Madden, P. Luke, and J. Walton of the Instrument Science and Engineering Dept., LBL, for their advice and for the fabrication and modification of detectors and electronics, sometimes on a very short notice. These studies were supported by the National Cancer Institute under grant CA-15184, and the Department of Energy under contract DE-AC03-76SF00098.

REFERENCES

1. B. Crawford and D. Tuttle, private communication.
2. A. Chatterjee, C.A. Tobias, and J.T. Lyman, in Nuclear Fragmentation in Therapeutic and Diagnostic Studies with Heavy Ions, edited by Shen and Merker (Reidel, Dordrecht, Holland, 1976), 169.
3. E.A. Blakely, C.A. Tobias, T.C.H. Yang, K.C. Smith and J.T. Lyman, Radiat. Res. **8**, 122 (1979).
4. J.T. Lyman, in Proceedings IAEA Advisory Group Meeting on Advances in Dosimetry for Fast Neutrons and Heavy Charged Particles for Therapy Applications (Vienna, Austria, 1982). [Lawrence Berkeley Laboratory Report LBL-14779, 1982.]
5. P.L. Jain, Nuovo Cimento **8**, 839 (1959).
6. P.L. Jain, G. Das, B.T. Cheng and Y. Aliakbar, Phys. Lett. **88**, 189 (1979).
7. P.L. Jain and G. Das, Phys. Rev. Lett. **48**, 305 (1982).
8. P.L. Jain, private communication.
9. E.V. Benton, and R.P. Henke, Nucl. Instr. Methods **58**, 241 (1968).
10. E.V. Benton, R.P. Henke and C.A. Tobias, Science **182**, 474 (1973).
11. E.V. Benton, R.P. Henke, and C.A. Tobias, Nucl. Track Detec. **1**, 139 (1977).
12. E.V. Benton, R.P. Henke, R. Casson, G.T.Y. Chen, J. Llacer, W.R. Holley, T. Kanai, and J.T. Lyman, Med. Phys. **10**, 534 (1983) (Abstract).
13. W. Schimmerling, E.V. Benton, D.J. Hildebrand, R.P. Henke, W. Heinrich, and C.A. Tobias, in Biological and Medical Research with Accelerated Heavy Ions at the Bevalac, 1977-1980, LBL-11220, edited by M.C. Pirruccello and C.A. Tobias (Lawrence Berkeley Laboratory, Berkeley, 1980), 36.
14. W. Schimmerling, T.S. Subramaniam, W.J. McDonald, S.N. Kaplan, A. Sadoff and G. Gabor, Nucl. Instr. Methods, **205**, 531 (1983).

15. J. Llacer, E.E. Haller, W.I. Hansen, J.T. Walton and E. Batho, IEEE Trans. Nucl. Sci. **NS-28(1)**, 161 (1981).

16. J.B. Moulton, J.E. Stephenson, R.P. Schmitt and G.J. Wozniak, Nucl. Instr. Methods **157**, 325 (1978).

17. B. Rossi, High Energy Particles, (Prentice Hall, New York, 1952), Chapter 2.

18. S. M. Seltzer and M.J. Berger, in Studies in Penetration of Charged Particles in Matter, National Academy of Science - National Research Council publication 1133.

19. B.D. Maccabee, Radiat. Res. **54**, 495 (1973).

20. B.D. Maccabee and M.A. Ritter, Radiat. Res. **60**, 409 (1974).

21. F.S. Goulding and B.G. Harvey, Ann. Rev. Nucl. Sci. **25**, 167 (1975).

22. W. Schimmerling and S.B. Curtis, Radiat. Res. **72**, 1 (1977).

23. D.F. Greiner, Nucl. Instr. Methods

24. J. Llacer, IEEE Trans. Nucl. Sci. **NS-28(1)**, 630 (1981).

25. P.J. Lindstrom, D.E. Greiner, H.H. Heckman, B. Cork, and F.S. Bieser, Proceedings, 10th International Cosmic Ray Conference, Munich, 1975, 2315.

26. C.W. Townsend, J.W. Wilson, and H.B. Bidasania, NASA Tech. Paper, 2138, (1983).

27. E.D. Cashwell and C.J. Everett, A Practical Manual for the Monte Carlo Method for Random Walk Problems (Pergamon Press, New York, 1959), Chapter 10.

This report was done with support from the Department of Energy. Any conclusions or opinions expressed in this report represent solely those of the author(s) and not necessarily those of The Regents of the University of California, the Lawrence Berkeley Laboratory or the Department of Energy.

Reference to a company or product name does not imply approval or recommendation of the product by the University of California or the U.S. Department of Energy to the exclusion of others that may be suitable.

TECHNICAL INFORMATION DEPARTMENT
LAWRENCE BERKELEY LABORATORY
UNIVERSITY OF CALIFORNIA
BERKELEY, CALIFORNIA 94720